



HIGH RESOLUTION AIRBORNE THERMAL INFRARED REMOTE SENSING STUDY, SILALI GEOTHERMAL PROSPECT, KENYA

J. Mutua¹, A. Friese², F. Kuehn², T. Lopeyok¹, M. Mutonga¹ and N. Ochmann²

¹Geothermal Development Company

P.O. Box 17700-20100, Nakuru

KENYA

jmutua@gdc.co.ke

²The Federal Institute for Geosciences and Natural Resources

Geozentrum Hannover, Stilleweg 2, D-30655, Hannover

GERMANY

Andrea.Friese@bgr.de

ABSTRACT

Airborne high-resolution thermal infrared (TIR) remote sensing has proven to be an effective method for mapping surface spatial temperature patterns. As geothermal energy continues to be a source of safe, reliable and renewable source of energy world over, TIR remote sensing has formed a key component of geothermal exploration. When combined with other spatial datasets, the TIR data showed areas of thermal influence resulting from geothermal activity associated with point, area and linear sources such as fumaroles, hot ground, fissures and faults. This paper describes the image acquisition and processing methodology, of high-resolution airborne thermography conducted over 2000 km² within the Silali geothermal prospect. The objective of the study was to characterize the geothermal features for further focused geothermal exploration studies.

1. INTRODUCTION

Thermal infrared (TIR) remote sensing provides data with synoptic coverage for investigating the surface manifestations of geothermal systems as applied to both geothermal energy exploration and also for more fundamental research and monitoring. TIR remote sensing provides a method for rapid mapping and quantifying surface geothermal features in support of exploration and assessment of new resources (Eneva et al., 2006; Kratt et al., 2006; Coolbaugh et al., 2007; Eneva et al., 2007; Rockwell and Hofstra, 2008; Kienholz et al., 2009; Littlefield and Calvin, 2009; Scherer et al., 2009; Taranik et al., 2009; Littlefield and Calvin, 2010; Haselwimmer et al., 2011; Reath and Ramsey, 2011).

Airborne thermal infrared remote sensing is a proven method of obtaining high-spatial resolution thermal imagery. Several applications using thermal imagery can be found in the literature. For example, Torgersen et al, 2001, used airborne thermal remote sensing to assess water temperatures in rivers and streams, related to fisheries habitat. Quattrochi and Luvall, 2003 presented several applications using airborne and satellite based thermal infrared applications to retrieve surface parameters and processes. This project was undertaken in Silali geothermal prospect in the Northern sector of the Kenyan Rift as shown in Figure 1. Previous integrated geophysical, geological and geochemical studies in the area (Lagat et al.,2010, Dunkley et al.,1993), indicated existence of a geothermal resource under Silali caldera which extends to the eastern flanks of the volcano. The results

signified probable occurrence of a high temperature geothermal resource and recommended the prospect for further detailed investigations to determine its resource potential.

2. DATA COLLECTION

2.1 Description of the airborne remote sensing system

For this survey, a DigiTHERM thermal camera system was used (Figure 2). DigiTHERM is a camera developed for professional digital aerial thermography (IGI, 2013).

Its core component is an Infratec VarioCAM with 640 x 480 pixel field of view and 7.5 to 14 μm wavelengths and 30 mm focal length (InfraTec, 2013). With thermal resolution of 0.05K, the camera senses temperature in the range from -40°C to 1200°C . The uncooled microbolometer FPA-detector delivers thermal images in system-specific *.irb format. A graphical user interface allows real time preview and check of recorded thermal images.

The camera was mounted in a nadir looking position on a high-grade aluminum/carbon composite installed through a portal in the belly of a two engine Piper PA-31 Turbo Navajo aircraft chartered from Photomap International Ltd. (Andrea et al., 2012).

The thermal camera was operated via graphical user interface running on touch screen monitors (Figure 3) connected to the DigiCONTROL Sensor Management Unit (SMU). The raw thermal information was stored in 240GB Solid State Devices (SSD). For precise determination of position and altitude of the airborne sensor at the instant of exposure, the AERO control system used an Inertial Measurement Unit (IMU) for post acquisition georeferencing, orthorectification and mosaicking of the individual thermal images.

2.2 Image acquisition

High resolution thermal infrared images were recorded over an area of 2000 km^2 over the Silali geothermal prospect. A total of 32 flight lines each 50 km long were planned to ensure 25% side lap and 80% forward lap to guarantee complete coverage of the study area as shown in Figure 4. Other parameters are as outlined in Table 1.

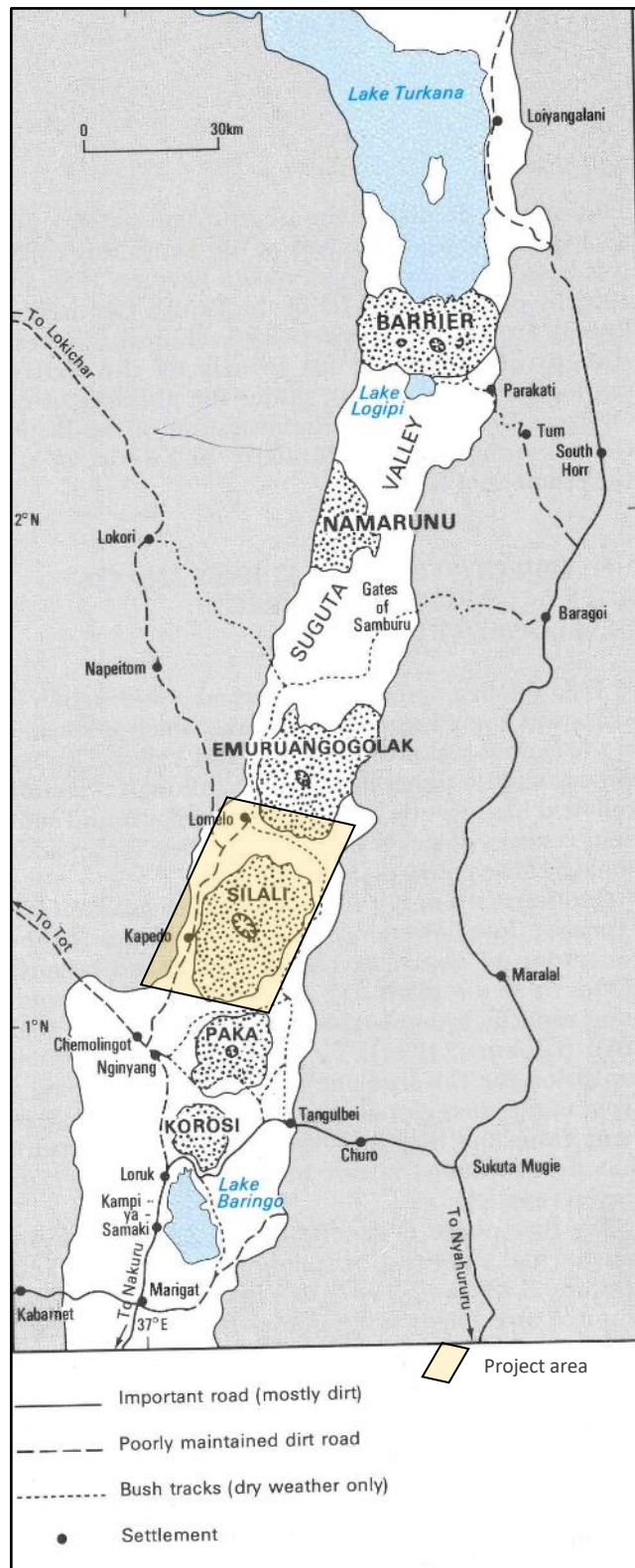


FIGURE 1: Map of the northern sector of the Kenya Rift showing the project area (modified from Dunkley et al., 1993)

In order to minimize influence of sun-dependent heating of the ground surface during daytime, the image acquisition over-flights were conducted during the second half of the night time hours (3:00 am to 6:00 am) and under clear sky conditions from 26th to 28th January 2012. This was to ensure that the thermal images are recorded at a time when the radiative cooling of the surface has been attained. Reference temperature thermal images and infrared thermometer measurements were carried out at Lake Baringo where surface water temperatures were recorded at hourly intervals on 28th January in the same site where a reference flightline of thermal images was also recorded.

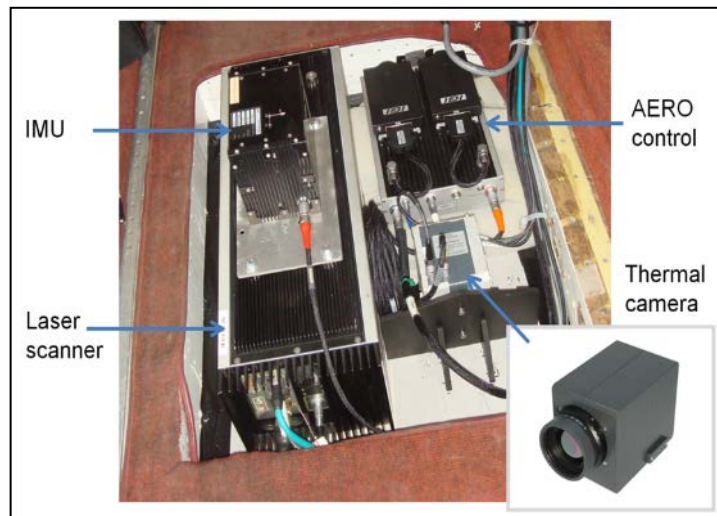


FIGURE 2: Thermal system equipment layout in the aeroplane



FIGURE 3: Touch screen monitors for operating the Thermal camera and the camera hatch as seen from below the aeroplane

3. IMAGE PROCESSING

The individual spectral images from the DigiTHERM camera was stored in system specific format “*.irb” at a mean of 3-meter pixel resolution. Pre-processing was conducted for all the raw thermal images and calculation of orientation parameters for every single thermal image with IGI AERO office software with input data been the IMU records. After conversion of all raw thermal images to 8 bit and 16 bit *.tiff, direct geo-referencing of all single thermal images was done. This was followed the procedures outlined below:

- a. Mosaicking of all 6,236 single ortho thermal images with automatic calculation of seam lines but without radiometric correction of camera lens' vignetting; resulted in ortho thermal image mosaic (16 bit *.GeoTiff format) with visible seam lines. The mosaic was radiometrically unaltered and served as base for further temperature calibrations (step b).

- b. From radiometrically uncorrected mosaic, the 16 bit digital number values of the mosaic's pixels were transformed to temperature ranges using temperature range function developed from relationship of image digital numbers and reference temperatures measurements (Figure 5). The result was a mosaic of thermal images, in which pixel values represented the surface temperatures.
- c. In a parallel processing line, radiometric correction was applied in order to avoid visible seam lines. The output format was a 16 Bit GeoTiff. This mosaic showed a balanced grayscale distribution controlled by temperature relations but not absolute temperatures.

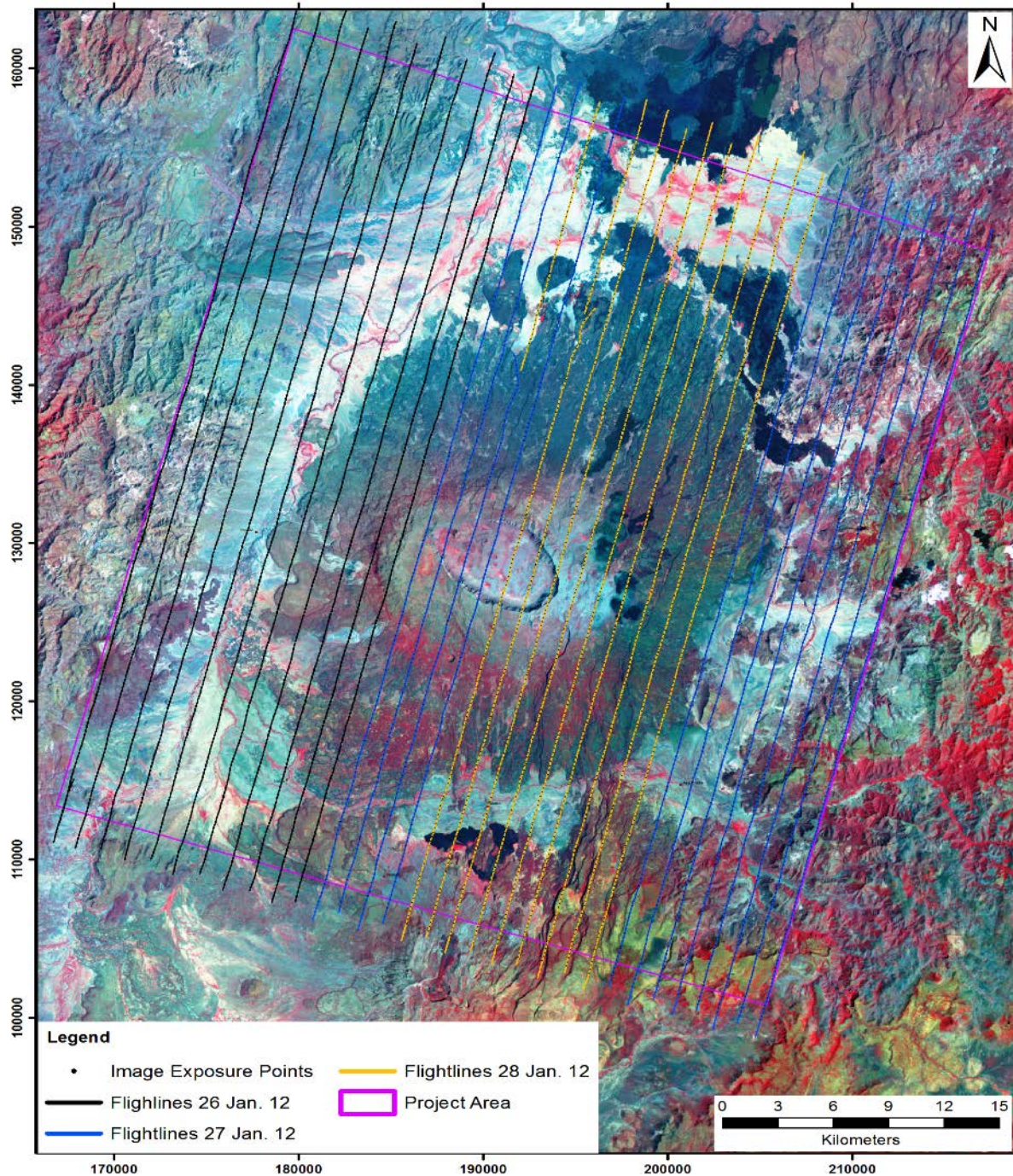


FIGURE 4: Landsat TM image (bands 421, RGB)

TABLE 1: Key survey parameters

Survey parameters	Value
Altitude above ground	3,600 m
Flight altitude above mean sea level	4,500 m
Number of flight lines	32
Length of flight lines	50 km
Distance between flight lines	1,340 m
Distance between midpoints two thermal images	270 m
Mean GSD (ground sampling distance/ pixel size)	3 m
Field of view per image	1920 m by 1440 m
Number of triggered raw thermal images	6,236

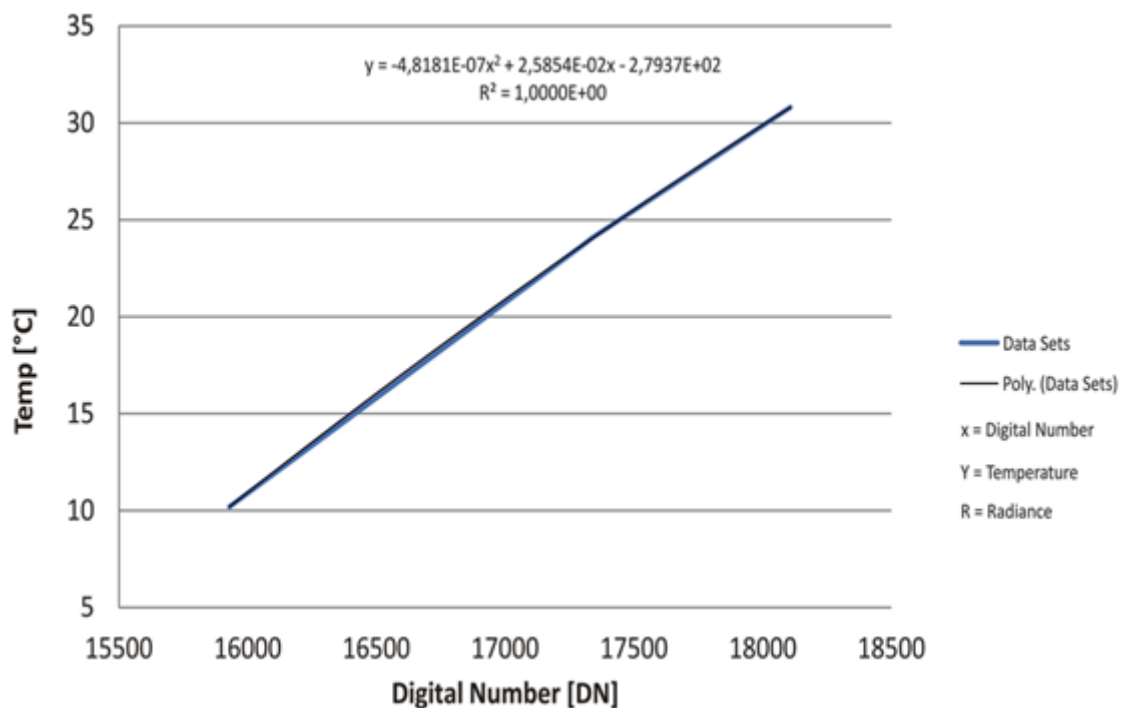


FIGURE 5: Temperature range function developed to convert 16 bit digital number values of pixels of single thermal images and of thermal mosaic to temperature values

4. RESULTS AND DISCUSSION

From the mosaicked thermal images more than 1000 thermally anomalous areas were identified from automatic screening. This outlined areas which were considered for further analysis of individual or smaller mosaics of thermal images and validated through field visits.

4.1 Analysis of single/mosaicked images of selected sites

Using the single thermal images or small scale mosaics of the anomalous areas as obtained from the automatic screening, detailed analysis gave more insights into these thermally anomalous areas as outlined below for areas A and B outlined in Figure 6.

Fumarole field SF 5 before was known as single “hot spot”. The measured temperature of fumarole SF 5 was 80°C, this showed the averaging of temperatures of the ground cells covered by pixel of a single thermal image. However, the thermal image revealed that SF 5 is a very complex system and not a

single feature, most probably (Figure 7). Five nearly linear thermal features were recognizable on the thermal image (solid white arrows; dashed white arrows for indistinct lineament). The area of thermally anomalous temperatures is 1.0 km by 0.5 km wide. Highest pixel temperature of 18.15°C was recorded at E 191538 N 129837. General surface temperature of surrounding area was between 10 to 11°C. Areas with pixel temperatures higher than 14.20°C are highlighted on the thermal image and spot image (Figure 8) and show the whole extend of the system.

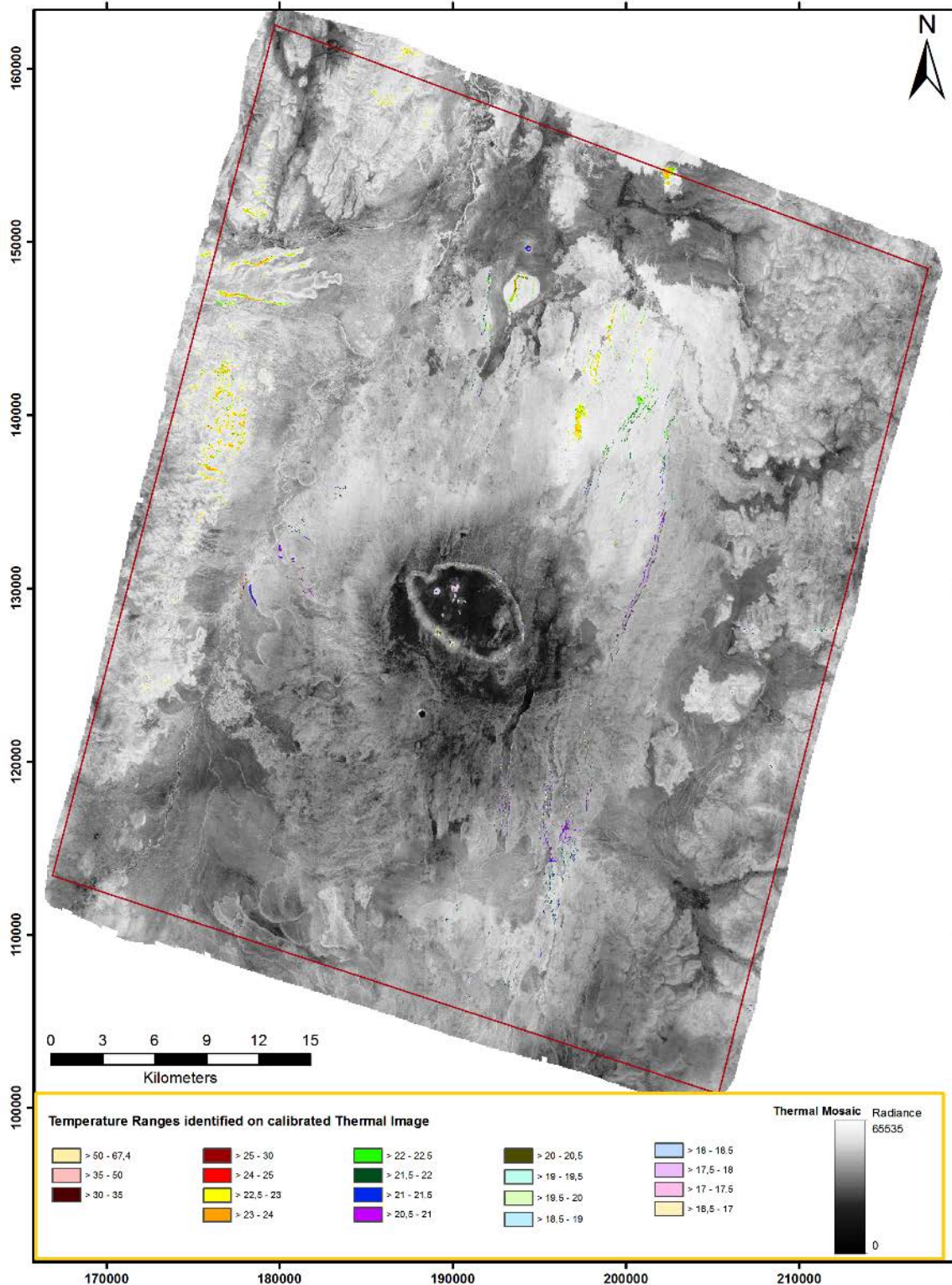


FIGURE 6: Thermal anomalies from the mosaicked image

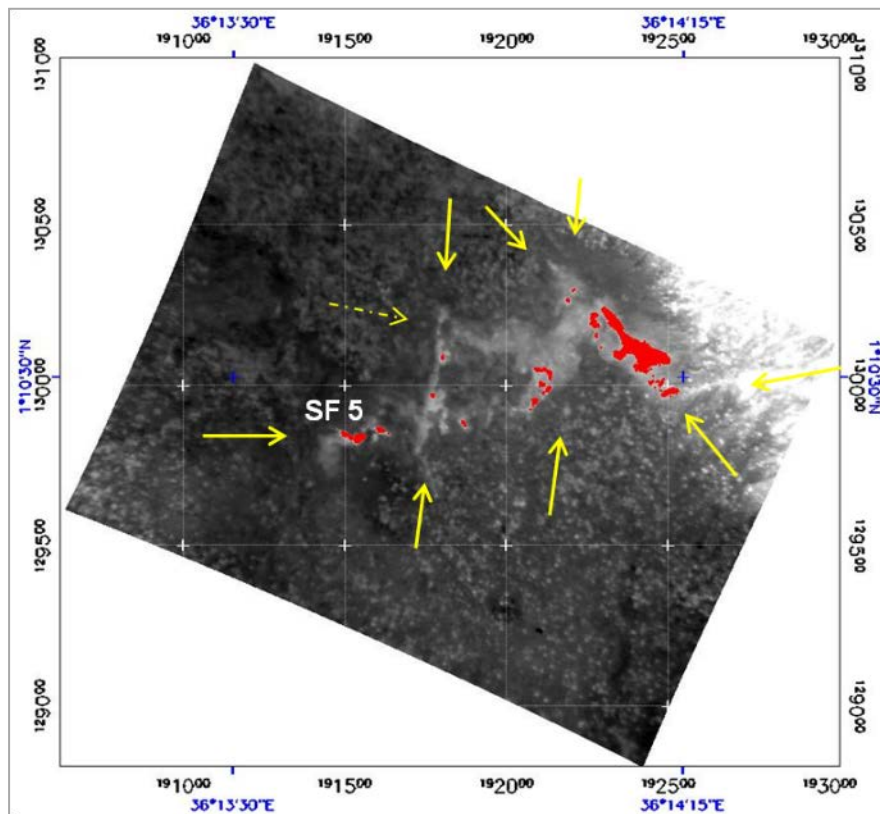


FIGURE 7: Thermal ortho-image of Area A

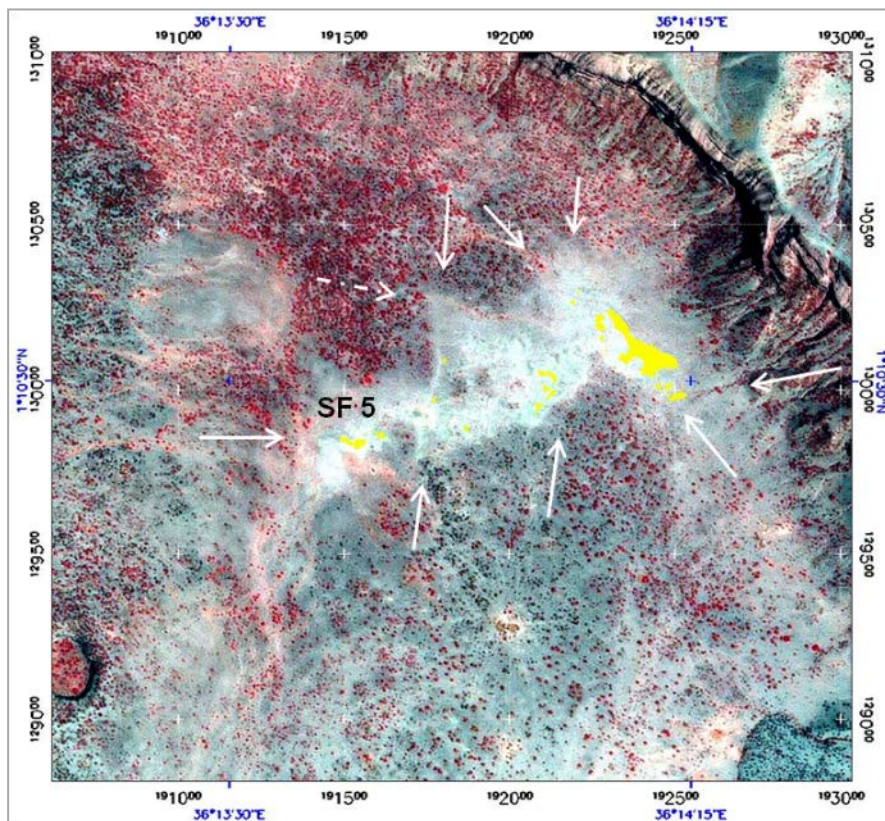


FIGURE 8: Thermal anomalies over Spot 5 image of Area A

The area marked on the thermal image (Figures 9 and 10) showed the highest pixel temperatures of 18°C and area marked b also showed elevated temperatures of 15°C to 16°C. The highest temperature was measured directly at a junction of two linear features (marked with B) and the others outlined by the arrows. The thermal anomalies followed the dense NNE-SSW trending fault lines and fissures in this area. Therefore, we suppose that the linear fault lines and fissures are the conduits of the recorded thermal anomalies in this region associated with magma at depth. This approach was applied for the different thermal anomalies identified after the thermal screening for in-depth understanding.

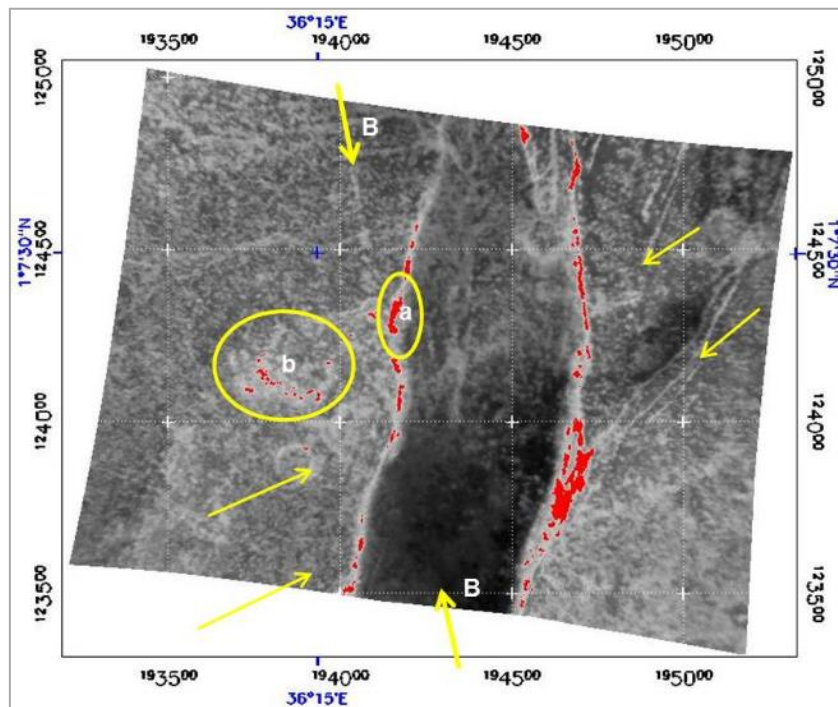


FIGURE 9: Thermal ortho-image of Area B

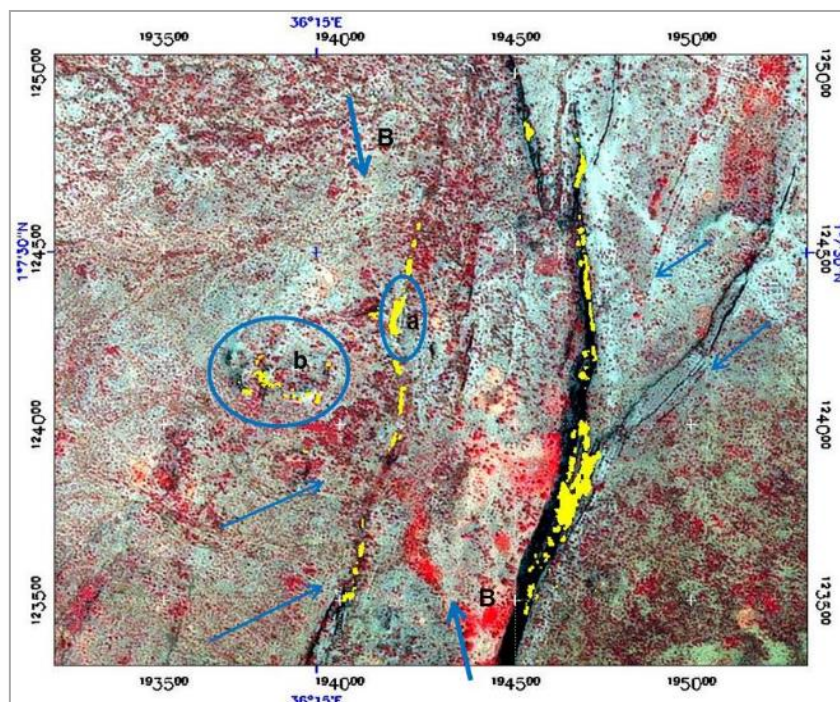


FIGURE 10: Thermal anomalies over Spot 5 image of Area B

5. CONCLUSIONS

Airborne thermal infrared remote sensing has the flexibility to provide imagery with reasonably high spatial resolution which was valuable in locating unidentified thermal anomalies in Silali geothermal prospect. Thermal anomalies in the Eastern flanks of the caldera was mapped which was found to be related with the intense fissures and fault system in the area. Also already known fumaroles and hot grounds were revealed from the thermal survey that they covered extensive areas that known before. The discovered thermal anomalies complemented earlier exploration works in the area and helped in characterizing surface thermal anomalies and understanding of thermal relationships that were not known before. The use of high resolution TIR remote sensing was not separated from other aspects of science (geology, geochemistry, and geophysics). Therefore, TIR remote sensing provided a unique tool for qualitative and quantitative initial investigations contributing to detailed geothermal exploration surveys in geothermal exploration. The surface geothermal activity from TIR was also used to refine the interpretation and conceptualization of results from other exploration approaches. The obtained airborne TIR data will also be used to support long term monitoring of geothermal system in the prospect by providing repeatable method of inventorying surface geothermal features.

ACKNOWLEDGEMENTS

The project is part of the "GEO THERM programme - Promoting the Utilization of Geothermal Energy in Developing Countries", initiated and financed by the German Federal Ministry for Economic Cooperation and Development (BMZ). It was executed by the Federal Institute for Geosciences and Natural Resources (BGR) and Kenya's Geothermal Development Company (GDC)

REFERENCES

- Andrea, F., Kuehn, F., and Ochmann, N., 2012: *High-resolution thermal infrared remote sensing for geothermal site characterization of the Silali area, Northern Kenya Rift*. Project report.
- Coolbaugh, M.F., Kratt, C., Fallacaro, A., Calvin, W.M., and Taranik, J.V., 2007: Detection of geothermal anomalies using Advanced Spaceborne Thermal Emission and Reflection Radiometer (ASTER) thermal infrared images at Bradys Hot Springs, Nevada, USA. *Remote Sensing of Environment*, 106-3, 350-359.
- Dunkley, P.N., Smith, M., Allen, D.J., and Darling, W.G., 1993: *The geothermal activity and geology of the northern sector of the Kenya Rift Valley*. British Geological Survey, Research Report SC/93/01, 202 pp.
- Eneva, M., Coolbaugh, M., and Combs, J., 2006: Application of satellite thermal infrared imagery to geothermal exploration in East Central California. *GRC Transactions*, 30, 407-411.
- Eneva, M., Coolbaugh, M.F., and Bjornstad, S.J., 2007: In search for thermal anomalies in the Coso geothermal field (California) using remote sensing and field data. *Proceedings of the 32nd Workshop on Geothermal Reservoir Engineering*, Stanford University, Stanford, California, United States, 7 pp.
- Haselwimmer, C.E., Prakash, A., and Holdmann, G., 2011: Geothermal exploration at Pilgrim Hot Springs, Alaska using airborne thermal infrared remote sensing. *GRC Transactions*, 35, 805-810.
- IGI, 2013: *DigiTHERM*. Ingenieur - Gesellschaft für Interfaces mbH, Website: <http://www.igi.eu/digitherm.html>

InfraTec, 2013: Thermography – Infrared camera series. VarioCAM. Website: <http://www.infratec.de/en/thermography/infrared-camera.html>

Kienholz, C., Prakash, A., and Kolker, A., 2009: Geothermal exploration in Akutan, Alaska, using multitemporal thermal infrared images. *American Geophysical Union, Fall Meeting 2009*, abstract #H53F-1009.

Kratt, C., Calvin, W., and Coolbaugh, M., 2006: Geothermal exploration with Hymap hyperspectral data at Brady–Desert Peak, Nevada. *Remote Sensing of Environment* 104-3, 313-324.

Lagat, J., Mutoria, C., Wanjie, C., Mwakirani, R. et al., 2010: *Silali prospect: investigations for its geothermal potential*. Geothermal Development Company (GDC), Nairobi, Kenya, unpublished report.

Littlefield, E. and Calvin, W., 2009: Remote sensing for geothermal exploration over Buffalo Valley, NV. *GRC Transactions*, 33, 495-499.

Littlefield, E. and Calvin, W., 2010: Geothermal exploration using AVIRIS remote sensing data over Fish Lake Valley. *GRC Transactions*, 34, 599-603.

Quattrochi, D.A and Luvall, J.C., 2003: *Thermal remote sensing in land surface processes*. CRC Press, Boca Raton, Florida, United States, 464 pp.

Reath, K.A. and Ramsey, M.S., 2011: Hyperspectral thermal infrared analysis of the Salton Sea, CA geothermal field. *American Geophysical Union Fall Meeting 2011*, San Francisco, United States.

Rockwell, B.W. and Hofstra, A.H., 2008: Identification of quartz and carbonate minerals across northern Nevada using ASTER thermal infrared emissivity data — Implications for geologic mapping and mineral resource investigations in well-studied and frontier areas. *Geosphere* 4-1, 218-246.

Scherer, G.J., Riley, D.N., Peppin, W.A., Tratt, D.M., Wright, C., and Jones, K.L., 2009: Geothermal exploration with visible through long wave infrared imaging spectrometers. *Clean Technology Conference and Expo 2009*, Houston, Texas, United States.

Taranik, J.V., Coolbaugh, M.F., and Vaughan, R.G., 2009: An overview of thermal infrared remote sensing with applications to geothermal and mineral exploration in the Great Basin, Western United States. In: Bedell, R., Crosta, A., and Grunsky, E. (ed.), *Remote sensing and spectral geology. Reviews in Economic Geology*, vol. 16. Society of Economic Geologists Inc., Littleton, Colorado, United States, 18 pp.

Torgersen, C.E., Faux, R.N., McIntosh, B.A., Poage, N.J., and Norton, D.J., 2001: Airborne thermal remote sensing for water temperature assessment in rivers and streams. *Remote Sensing of Environment*, 76, 386-398.